Case Studies in Construction Materials 24 (2026) e06026

Contents lists available at ScienceDirect

Case Studies in Construction Materials

journal homepage: www.elsevier.com/locate/cscm

Replacing conventional activators with a waste-glass-derived dry alkaline activator for sustainable one-part geopolymer composites

Seemab Tayyab [a], Wahid Ferdous [a,*], Weena Lokuge [a], Tuan Ngo [b], Andreas Gerdes [c], Allan Manalo [a]

[a] University of Southern Queensland, School of Science, Engineering and Digital Technologies, Centre for Future Materials (CFM), Toowoomba, QLD 4350, Australia
[b] Department of Infrastructure Engineering, The University of Melbourne, VIC 3010, Australia
[c] Karlsruhe Institute of Technology (KIT) Innovation HUB–Prävention im Bauwesen Ein Helmholtz Innovation Lab, Hermann-von-Helmholtz-Platz 1, Germany

ARTICLE INFO

Keywords:
One-part geopolymer composites
Dry alkaline activators
Thermochemical activation
Waste glass powder
Taguchi optimisation
Sustainable construction

ABSTRACT

One-part geopolymer concrete (GPC) offers a safer and more sustainable alternative to conventional alkali activation by eliminating hazardous liquid alkaline solutions. This study presents a novel thermochemical approach for synthesising a dry alkaline activator (DA) using waste glass powder (WGP). The effects of SiO_2/Na_2O molar ratio (Ms = 0.5, 1.5, 2.5), activation temperature (T of 150–350 °C), duration (t of 1–3 h), and water dosage (w of 0–10%) were investigated using a Taguchi design of experiments. FTIR and SEM-EDS analyses confirmed sodium silicate formation, with optimum efficiency (80%) achieved at Ms = 1.5, 150 °C, 2 h, and 10% water. This optimised DA was used to produce one-part geopolymer (GP) composite mixes at different DA/binder ratios (0.3–0.5), which were tested for rheological, mechanical, and microstructural properties. Rheological characterisation revealed shear-thinning behaviour with elastic-dominant viscoelasticity. Compressive strength increased with activator dosage, reaching up to 24.5 MPa after 28 days, under heat curing for 24 h, surpassing that of liquid-activated GPC. Sustainability analysis revealed up to 68% CO_2 and 57% cost reduction compared with conventional GPC. Overall, the findings demonstrate the feasibility of waste-glass-based dry activators as a cleaner, safer, and economically viable alternative for scalable one-part GP production aligned with circular economy principles.

1. Introduction

1.1. Background

The global construction sector is increasingly under pressure to reduce its environmental footprint, with ordinary Portland cement (OPC) production accounting for approximately 8% of global CO_2 emissions [1]. In response, alkali-activated materials (AAMs) have emerged as promising substitutes because of their lower embodied carbon and capacity to incorporate industrial by-products such as

* Corresponding author.
E-mail addresses: Seemab.Tayyab@unisq.edu.au (S. Tayyab), Wahid.Ferdous@unisq.edu.au (W. Ferdous), Weena.Lokuge@unisq.edu.au (W. Lokuge), dtngo@unimelb.edu.au (T. Ngo), andreas.gerdes@kit.edu (A. Gerdes), Allan.Manalo@unisq.edu.au (A. Manalo).

https://doi.org/10.1016/j.cscm.2026.e06026
Received 24 December 2025; Received in revised form 5 March 2026; Accepted 26 March 2026
Available online 27 March 2026

Table 1
Oxide compositions of FA and WGP.

	SiO_2	Al_2O_3	Fe_2O_3	CaO	SO_3	MgO	Na_2O	K_2O	LOI
Fly ash	51.48	28.39	6.93	5.42	0.09	1.10	0.15	0.53	0.03
WGP	70.1	3.5	1.23	11	0.35	0.5	12	0.7	1.3

Note: All values in mass%, expressed on an oven-dry basis; LOI: loss on ignition at 1000 °C.

fly ash (FA), slag, and metakaolin [2]. Within the broader class of AAMs, GP systems formed through the alkaline activation of aluminosilicate-rich materials [3] have garnered significant attention for their mechanical performance, chemical resistance, and long-term durability [4–6]. It is gaining popularity for usage in civil infrastructure, including airport pavements (Brisbane Well Camp Airport), academic buildings (Global Change Institute at the University of Queensland, Australia), retaining walls, marine structures, bridge decks, and even in 3D printed elements [7–9]. Despite the significant environmental and performance advantages of GP technology, its widespread implementation, particularly in cast-in-situ applications, remains limited. A key barrier on the adoption of GP technology is the dependence on corrosive and highly viscous liquid alkaline activators, such as sodium hydroxide and commercial sodium silicate solutions [10,11]. The liquid introduces serious handling and safety dangers, require specialised storage and transportation, and have a limited shelf life. Moreover, their preparation and on-site mixing demand strict quality control procedures, which are often impractical at the construction scale and introduce variability in performance. From a sustainability perspective, the production of liquid sodium silicate is particularly carbon-intensive, involving the high-temperature calcination of sodium carbonate with silica sand, which contributes significantly to CO_2 emissions [12]. Although AAMs have been shown to reduce greenhouse gas emissions by 32–64% compared to conventional OPC concrete of equivalent strength, it is noteworthy that the alkaline activators themselves, primarily hydroxides and silicates, account for approximately 60% of the total environmental burden of AAMs [13]. In response to these challenges, the development of "one-part" or "just-add-water" GP binders has emerged as a promising alternative. In these systems, solid activators are pre-mixed with aluminosilicate precursors, enabling simplified handling, improved safety, and enhanced consistency during field application. This approach significantly enhances the practicality and scalability of GP technology for structural and commercial use.

Most one-part GP systems currently rely on commercially manufactured solid sodium silicate-based activators, which are energy-intensive, costly, and often not locally available [14]. To address this issue, recent studies have explored the feasibility of synthesising DA from silica-rich waste-derived sources via a thermochemical process (transforming waste materials into reactive solid-state activators by combining them with sodium hydroxide and applying controlled thermal treatment, resulting in sodium silicate-rich phases capable of activating aluminosilicate precursors) [13,15–22]. Among these, WGP has demonstrated high potential due to its abundant availability, high silica content, and underutilisation in high-value construction applications.

WGP has been extensively investigated in cementitious and GP systems. Previous studies have explored WGP as a supplementary cementitious material [23–25], partial precursor replacement [15,26–29], or filler to improve mechanical and durability performance. Studies have also summarised the roles of WGP and process parameters affecting GP behaviour, highlighting its pozzolanic reactivity and sustainability benefits [26]. More recent works have examined WGP-based GP composites under thermal or mechanical loading, as well as predictive modelling of oxide ratios in GP formation [30,31]. However, most of these studies focus on WGP as a precursor or additive rather than as a thermochemically synthesised DA capable of replacing commercial sodium silicate in one-part systems. Moreover, systematic multi-parameter optimisation of dry activator synthesis-considering silica modulus, temperature, duration, and water dosage simultaneously-remains largely unexplored. In particular, the literature lacks statistically robust optimisation frameworks linking activator synthesis efficiency directly to rheological behaviour, mechanical performance, and cradle-to-gate sustainability assessment. This study addresses this gap by integrating thermochemical activator synthesis with Taguchi-ANOVA optimisation and performance validation in one-part GP composites.

1.2. Novelty and significance of the study

The significance of this study lies in developing a fully waste-derived DA that replaces conventional caustic liquid activators in one-part GP production. The novelty of this work does not lie solely in the application of the Taguchi method, but in the integrated framework combining: (i) thermochemical synthesis of a fully waste-derived dry activator, (ii) statistically guided multi-parameter optimisation using Taguchi-ANOVA analysis, (iii) semi-quantitative evaluation of sodium silicate formation efficiency, and (iv) direct correlation of activator efficiency with rheological, mechanical, microstructural, and sustainability performance in one-part GP composites. The present study addresses important fundamental research questions: (i) Can a sodium silicate-rich DA be efficiently synthesised from WGP using a thermochemical process? (ii) How do key design parameters molar ratio, activation temperature, duration, and water dosage, govern the yield and quality of the DA? (iii) Can the performance of the resulting activator be reliably predicted and optimised using Taguchi-based statistical tools, and (iv) How does the optimised DA influence the fresh, mechanical, microstructural, and sustainability characteristics of one-part GP composites compared to conventional systems? To answer these questions, this study adopts a multi-phase approach that encompasses DA synthesis via the thermochemical method, process optimisation through Taguchi design of experiments, material characterisation using FTIR and SEM-EDS, and composite performance evaluation by mechanical, rheological, and microstructural analysis, including sustainability and economic assessments.

Fig. 1. Procedure steps to produce the activating powder.

Table 2
Selected design parameters and their levels.

Parameters (D_p)		Levels (l)		
		1	2	3
A	SiO_2/Na_2O ratio	0.5	1.5	2.5
B	Temperature (°C)	150	250	350
C	Duration (hrs.)	1	2	3
D	Water* (%)	0	5	10

Note: * % by mass of dry activator.

2. Materials and methods

2.1. Raw materials

This study used materials sourced from the industrial waste stream for their potential as a reactive agent in the manufacture of a DA. WGP was obtained from post-consumer soda-lime glass, which was subsequently cleaned, dried, and finely milled to a particle size of less than 75μm. X-ray fluorescence (XRF) analysis verified a silica concentration over 70 wt%. Table 1 presents the major oxide composition of the materials.

A mixture of sodium hydroxide pellets and sodium silicate solutions was used as an alkaline activator to make conventional GP composites for comparison purposes. Chem-Supply Pty Ltd., Australia, supplied sodium hydroxide (98.0% purity). The commercial sodium silicate solution supplied by Sigma-Aldrich Australia had the following composition: 14.7% Na_2O, 29.4% SiO_2, and 55.9% water (by weight). The waste-derived DA was prepared using sodium hydroxide with WGP through the thermochemical method described in Section 2.2.1.

Class F fly ash (FA) was used as the main aluminosilicate precursor for the GP composite matrix. It complied with ASTM C618 [32] and exhibited > 50 wt% of $SiO_2 + Al_2O_3 + Fe_2O_3$. Locally available river sand with a fineness modulus of 2.71 was used as fine aggregate. Deionised water was used for all activator mixing and specimen casting.

2.2. Methods

The experimental work was structured in three sequential phases: synthesis of DA via thermochemical treatment (Phase I), efficiency based on silica availability and structural features, and optimisation using Taguchi design of experiment (Phase II), and evaluation of one-part GP composites prepared using the optimised DA (Phase III).

2.2.1. Synthesis of DA via thermochemical method

The DA was prepared via the thermo-chemical method (shown in Fig. 1) as suggested in existing research [16,33], by mixing WGP as SiO_2 source with sodium hydroxide pellets as Na_2O source by varying different parameters influencing the activator's efficiency, such as molar ratio, heating temperature, heating period, and water dosage. During the heat treatment, the synthesis of sodium silicate occurred following the reaction given in Eq. (1) [34]. The resulting solid material was subsequently pulverised into a powder using a 75 μm sieve after a ball mill. A total of 100 g of powder was prepared by mixing sodium hydroxide with silica-rich source at target molar ratios. The mass of the SiO_2-rich source and sodium hydroxide proportions was calculated based on the known SiO_2 and Na_2O content of each. The molar masses of SiO_2 and Na_2O (60.08 g/mol and 61.98 g/mol, respectively) were used to convert the target molar ratio into a mass-based mixing ratio for each combination. The required moles of Na_2O were first determined from the desired molar ratio using Eq. (2).

$$2NaOH + SiO_2 \xrightarrow{\Delta} Na_2SiO_3 + H_2O \quad (1)$$

$$Moles\ of\ Na_2O = \frac{wt\%\ \ of\ Si_2O * \ m_{p1}/100}{M_s} \quad (2)$$

where Ms is the desired SiO_2/Na_2O ratio, and m_{p1} is the mass of sodium hydroxide required. The corresponding required mass of silica-

Table 3
$L_9(3^4)$ orthogonal array used for experimental design.

Experiment No.	SiO_2/Na_2O ratio	Temperature (°C)	Time (hrs.)	Water (%)
E1	0.5	150	1	0
E2	0.5	250	2	5
E3	0.5	350	3	10
E4	1.5	150	2	10
E5	1.5	250	3	0
E6	1.5	350	1	5
E7	2.5	150	3	5
E8	2.5	250	1	10
E9	2.5	350	2	0

Fig. 2. Visual appearance of WGP–sodium hydroxide mixtures: (a) E1, (b) E4, (c) E7 before and (d) during thermal activation in muffle furnace.

rich source (m_{p2}) was then calculated by subtracting m_{p1} from the total mass of 100 g.

The Taguchi method [35] is an effective tool for designing experiments that can significantly reduce the number of tests required while retaining the effects of each variable on the final output. The design parameters considered in this study, along with their levels, are shown in Table 2. The molar ratio was varied across three levels (0.5, 1.5, and 2.5) to capture the transition from sodium-rich to silica-rich environments. The activation temperature levels of 150 °C, 250 °C, and 350 °C were selected based on the ability to initiate solid-state reaction without inducing vitrification or loss of reactive phases. Additionally, holding times of 1, 2, and 3 h were selected to examine the kinetic impact on sodium silicate development. Lastly, the incorporation of water (0, 5, and 10 wt% DA) was conducted to determine if water functions as a catalyst during the reaction. Similar ranges have been reported in past studies [16,20,22,33,36–39]. The required quantity of powders was mixed manually in sealed containers to ensure homogeneity, then subjected to thermal treatment in a muffle furnace at target temperatures and holding times. After heating, the powders were cooled in a desiccator to prevent carbonation and stored in airtight containers.

The minimum number of trials can be estimated using Eq. (3) to reduce experimental runs while maintaining statistical robustness, where D_p is the number of design parameters and l is the number of levels [40,41]. For four factors at three levels, this yields nine experiments, significantly fewer than the 81 required in a full factorial design, making the $L_9(3^4)$ orthogonal array an efficient and optimal choice. The corresponding trial combinations are presented in Table 3 [41,42] and the representative photographs of the WGP–sodium hydroxide mixtures prior to and during heat treatment are shown in Fig. 2.

$$\boldsymbol{n = 1 + (l - 1)D_p} \tag{3}$$

2.2.2. Efficiency of DA

The efficiency of each synthesised DA was evaluated based on its ability to form sodium silicate species, using a combination of Fourier Transform Infrared Spectroscopy (FTIR) and Scanning Electron Microscopy with Energy Dispersive X-ray Spectroscopy (SEM-EDS). These techniques provided both structural and compositional insights into the activation process. The phase characterisation in this study focuses on comparative efficiency assessment rather than comprehensive crystallographic identification. X-ray Diffraction (XRD) analysis was not conducted because the thermochemically synthesised powders exhibited predominantly amorphous characteristics, as indicated by the broad FTIR bands (Section 3.1, Fig. 4) and the absence of distinct crystalline features. Furthermore, the sodium silicate efficiency calculated from EDS-derived Na:Si molar ratios represent a semi-quantitative estimation rather than a direct phase quantification. The synthesised powders may contain a combination of amorphous and partially crystalline silicate species, and EDS does not distinguish between specific silicate phases. Therefore, the assigned stoichiometric compounds reflect the dominant theoretical phase based on elemental balance rather than exclusive single-phase formation. The adopted methodology is primarily intended for comparative evaluation across synthesis conditions. Future work incorporating complementary techniques such as XRD and quantitative phase analysis would provide more definitive phase identification and strengthen validation of the reaction products.

FTIR spectroscopy in transmission mode was conducted over the range of 4000–400 cm^{-1}, including Si–O–Si stretching (1000–1100 cm^{-1}), Si–O–Na (950–1000 cm^{-1}), indicative of sodium silicate [43], and O–H stretching (3200–3600 cm^{-1}) for hydrated

phases or unreacted sodium hydroxide (3640 cm^{-1}) [44,45]. Supporting peaks, such as those near 880–890 cm^{-1} (Si–OH bending) and 710–740 cm^{-1} (Si–O–Na), were used to confirm the presence of intermediate and final sodium silicate structures. The actual sodium silicate content in the synthesised DA powders was quantitatively estimated based on elemental analysis obtained through EDS [46]. For each sample, elemental analyses (EDS) were performed to determine the bulk Na (%) and Si (%) in each dry-activated powder sample. The corresponding Na:Si molar ratio was then calculated and used to infer the dominant sodium-silicate phase (e.g., Na_2SiO_3, Na_4SiO_4) and estimate the relative conversion of raw materials into reactive silicate gel. The use of this methodology has precedented from past studies to assess geo-polymerisation behaviour [47–49]. The methodology therefore provides a semi-quantitative indicator of activator efficiency and phase development. EDS spectra were collected from four randomly selected locations and averaged to determine the representative elemental mass percentages of Si, Na, O, and any impurities (e.g., Ca, Al, Fe, Mg, etc.).

2.2.2.1. Conversion to molar quantities. The averaged EDS values (in wt%) were converted to molar amounts per 100 g of powder using Eq. (4) [50].

$$\boldsymbol{n_{Na} \quad : \quad n_{Si}\,(molar) = wt.\ \%\frac{Na}{23} : wt.\ \%\frac{Si}{28}} \tag{4}$$

2.2.2.2. Stoichiometric assignment. The sodium silicate phase was assigned to each sample by comparing the molar ratio to known stoichiometries of common sodium silicates, e.g., Na_2SiO_3 (sodium metasilicate) = 2, $Na_2Si_2O_5$ (sodium disilicate) = 1, and Na_4SiO_4 (sodium orthosilicate) = 4, etc.

It is acknowledged that the EDS-derived Na:Si molar ratio provides a semi-quantitative estimation of sodium silicate formation. The thermochemically synthesised system may contain a combination of amorphous and partially crystalline silicate species rather than a single stoichiometric phase. Therefore, the assigned compound represents the dominant theoretical phase based on molar balance rather than exclusive phase purity. This approach enables comparative efficiency assessment across samples but does not imply complete single-phase formation.

2.2.2.3. Stoichiometric limiting reagent analysis. The required molar ratios of Na and Si were considered (e.g., 2:1 for Na_2SiO_3) for each assigned compound. The number of formula units that could be formed was calculated by identifying the limiting element among the available moles of Na and Si using Eq. (5).

$$\boldsymbol{n_{formula} = min \quad (\frac{n_{Na}}{x}, \quad \frac{n_{Si}}{y})} \tag{5}$$

where x and y are the stoichiometric Na: Si coefficients of the identified compound.

2.2.2.4. Yield calculation. The moles of sodium silicate units were multiplied by the molar mass of the assigned compound to obtain the total mass of sodium silicate formed in the powder using Eq. (6). Since the calculation was normalised to 100 g of sample, the resulting value directly represented the actual sodium silicate content in wt% using Eq. (7).

$$\boldsymbol{Mass_{compound} = n_{formula}\ x\ M_{compound}} \tag{6}$$

$$\boldsymbol{Yield \quad (\%) = \frac{Mass_{compound}}{Mass\ of\ sample}\ x\ 100} \tag{7}$$

where M is the molar mass of the assigned compound.

The optimisation was achieved using the Signal-to-Noise Ratio (SNR), based on the "larger-the-better" criterion (Eq. 8), where a higher SNR indicates better sodium silicate formation. SNR values were computed for all nine experiments, and the average SNR was determined for each level of the four factors. The optimal parameter combination was identified as the set yielding the highest average SNR.

$$\boldsymbol{SNR = \quad -10log_{10}(\frac{1}{n}\sum_{k=0}^{n}\frac{1}{y^2})} \tag{8}$$

where n = number of replicates, y_k = % sodium silicate yield for each run.

SNR analysis enables identification of optimal levels, but it does not quantify the contribution of each parameter. Therefore, Analysis of Variance (ANOVA) was used to determine the percentage influence of each factor based on the total variation in SNR. In orthogonal Taguchi designs where residual degrees of freedom are limited, contributions were estimated directly from SNR values using Eqs. (9–11):

$$\boldsymbol{Contribution_k = \quad \frac{SS_k}{SS_T}\ x\ 100} \tag{9}$$

$$\boldsymbol{SS_k = \quad \sum_{j=1}^{3} n\,(SNR_{kj} - \quad SNR_T)^2} \tag{10}$$

Table 4
Mix proportion (kg/m^3) of the one-part GP composites.

Sr #	Mix acronym	FA	Alkaline activator			Sand
			Sodium hydroxide	Sodium silicate	DA	
1	GPC-C	944	131.1	330.4	-	1590
2	GPC-DA0.3	647.5	-	-	277.5	
3	GPC-DA0.4	555	-	-	370	
4	GPC-DA0.5	462.5	-	-	462.5	

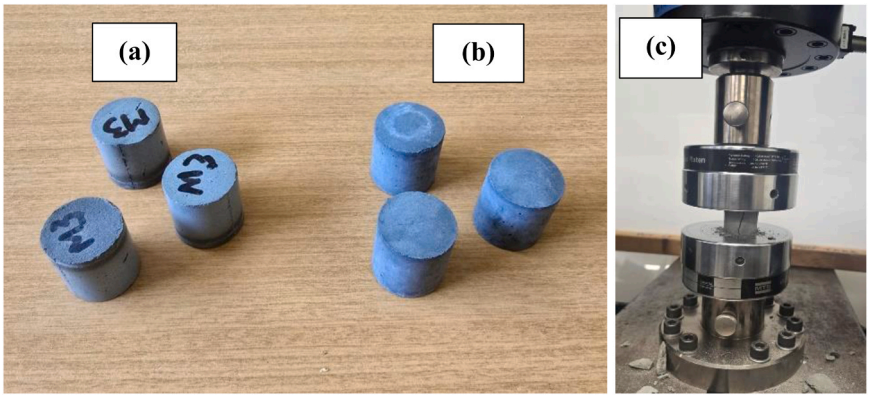

Fig. 3. Casting and testing of one-part geopolymer composites: (a) GPC-DA0.5, (b) GPC-C, and (c) compression testing.

$$SS_T = \sum_{i=1}^{9} (SNR_i - SNR_T)^2 \quad (11)$$

where SNR_{kj} is the average SNR for level j of parameter k, SNR_T is the grand mean of all SNRs, and n is the number of repetitions per level. SNR_i is the SNR value for the i^{th} experimental trial. This approach allows robust quantification of each parameter's effect, making it well-suited for Taguchi L_9 designs.

2.2.3. One-part geopolymer composites

2.2.3.1. Mix proportion. In Phase III, one-part GP composites were developed using the optimised DA from Phase II. The composite mix design involved systematic variation of the DA-to-binder ratios from 0.3 to 0.5 by mass, generating a matrix of mix combinations to evaluate rheological behaviour, workability, and mechanical performance. A batch of samples activated with a commercial sodium silicate and sodium hydroxide mixture was also created to compare with the alternatively activated samples. Materials were first dry-mixed (FA and DA) for 3 min to ensure uniform dispersion. Water was then added gradually with water-to-FA ratio of 0.35, and the mixture was blended for an additional 2 min to form a homogeneous paste [51]. Table 4 summarises the mix proportions (kg/m^3) used for each system.

2.2.3.2. Rheological measurements. The rheological properties of the WGP-based one-part GP paste were evaluated using a Modular Compact Rheometer (Anton Paar MCR series) equipped with a sandblasted concentric cylinder geometry. The inner radius of the cup cylinder was 15.16 mm, and the radius of the bob cylinder was 14.00 mm, resulting in a gap width of 1.16 mm [13,52]. All tests were conducted at a controlled temperature of 25 ± 0.5 °C. The paste was freshly mixed, and immediately after mixing, 20 g of the paste was poured into the cup cylinder.

A steady shear rate sweep was performed, ranging from 1 s^{-1} to 100 s^{-1} to measure shear stress and apparent viscosity. The Bingham plastic model (Eq. 12) was used to characterise flow behaviour:

$$\tau = \tau_0 + \tau_p.\dot{\gamma} \quad (12)$$

where τ is shear stress (Pa), τ_0 is yield stress (Pa), μ_p is plastic viscosity (Pa.s), and γ is shear rate (s^{-1}) extracted using linear regression. This test helped to evaluate the workability, static yield, and structural build-up of the GP matrix under flow.

An oscillatory frequency sweep to assess the elastic and viscous components of the paste was conducted over a range of 0.1–100 rad/s at a constant strain of 0.1%, within the linear viscoelastic region, determined through prior amplitude sweep testing. The measured parameters include G′ (storage modulus), G″ (loss modulus), and Tan δ (G″/G′). These properties were used to evaluate the fresh-state rigidity, structural build-up, and shape retention capacity of the paste, essential for casting and 3D-printing

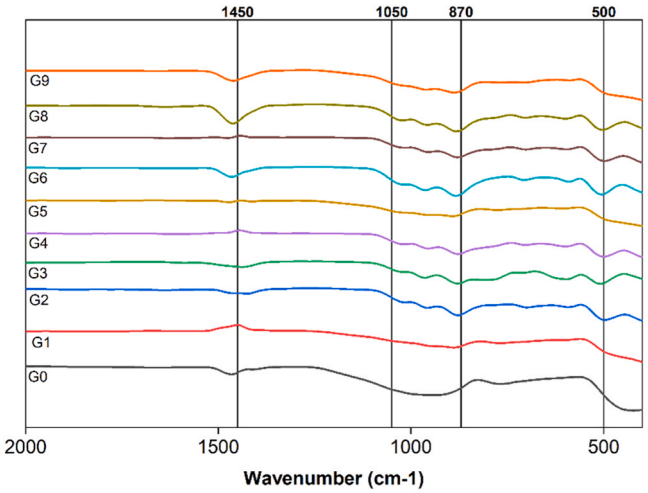

Fig. 4. FTIR spectra of DA derived from WGP.

Table 5
Qualitative assessment of sodium silicate formation in DAs.

Sample	Main Si-O peaks (cm^{-1})	Secondary peaks (cm^{-1})	Qualitative sharpness	Sodium silicate formation
E0	942.8	767.2, 422.1	Broad, unreacted	Baseline/ None
E1	888.9	768.7, 610.7	Broad, shifted left	Low
E2	957.1, 1014.4	698.9, 496.9	Emerging doublet	Moderate-High
E3	963.5, 1018.1	711.6, 508.7	Sharp, defined doublet	High
E4	955.9, 1019.2	703.1, 499.7	Sharp, slightly broadened	High
E5	952.6	604.8, 775.5	Single broad peak	Moderate
E6	962.7, 1017.3	706.4, 505.3	Very sharp twin peaks	Very High
E7	954.7, 1017.1	702.4, 497.8	Defined but weaker	Moderate-High
E8	958.3, 1022.2	702.7, 503.3	Slightly diffused	Moderate
E9	959.6	708.4, 589.1	Single moderate peak	Low-Moderate

Note: Peak assignments were validated against Refs [43–45,55–58].

applications. All rheological experiments were conducted in triplicate, and the averaged results were used for analysis.

2.2.3.3. Compressive strength. The fresh GP paste was cast into 25 mm diameter and 25 mm high cylindrical plastic pipe moulds, compacted on a vibrating table to eliminate entrapped air following the ASTM C579 method A [53]. The specimens were covered with plastic sheets for 24 hrs to prevent moisture loss, then demoulded and cured at 60 °C heat curing for 24 hrs and under ambient conditions (23 ± 2 °C and relative humidity >90%) until testing. Compressive strength was measured at 28 days of casting by ASTM C579 [54] using a 100 kN universal testing machine at a loading rate of 6000 psi (41 MPa/min). The casted specimen and sample subjected to compression are shown in Fig. 3. For selected mixes, SEM analysis was performed to assess the microstructure of the product.

3. Results and discussions

3.1. Development and characterisation of DA

The structural evolution of WGP-derived DAs was investigated using FTIR and SEM–EDS to establish the extent of sodium silicate formation. During thermochemical treatment, sodium hydroxide reacts with amorphous silica according to Eq. (1), leading to disruption of the –Si–O–Si– network and incorporation of sodium to form –Si–O–Na linkages [55].

Fig. 4 presents the FTIR spectra of the raw WGP and synthesised DAs. The untreated precursor (E0) exhibited a broad hump at 943 cm^{-1}, characteristic of amorphous silica. In contrast, activated samples developed distinct bands in the 950–1050 cm^{-1} region, associated with asymmetric Si–O–Si/Si–O–Al stretching and diagnostic of sodium silicate gels. Notably, E3, E4, and E6 showed sharp dual peaks at 962–963 cm^{-1} and 1017–1019 cm^{-1}, confirming the formation of highly polymerised sodium silicate phases. Secondary peaks at 500–600 cm^{-1} further supported Na–O–Si linkages. The qualitative assessment of sodium silicate formation in DAs is shown in Table 5. Broader or weaker features in E1, E5, E8, and E9 indicated incomplete activation or imbalanced silica modulus. The results demonstrate that intermediate SiO_2/Na_2O ratios (1.5) combined with moderate-to-high temperatures (250–350 °C) favour partial softening of the glass matrix and Na–Si–O gelation, whereas excessively Na-rich (Ms = 0.5) or Si-rich (Ms = 2.5) conditions led to

Table 6
Elemental composition (Si and Na), corresponding Na to Si molar ratio, assigned compound type, and equivalent sodium silicate efficiency of thermochemically synthesised DAs.

Exp. No.	Si (%)	Na (%)	Na: Si (molar)	Assigned compound	Limiting element	$Na_2Si_xO_y$ (%)	SNR (dB)
E0	23.3	8.38	0.44	Raw WGP	Na	39	-
E1	9.05	28.73	3.91	Na_4SiO_4	Si	56	34.96
E2	7.87	22.81	3.57	Na_4SiO_4	Si	53	34.48
E3	10.83	27.24	3.02	Na_2SiO_3	Si	59	35.42
E4	16.61	29.02	2.13	Na_2SiO_3	Si	80	38.06
E5	15.80	24.10	1.88	Na_2SiO_3	Si	78	37.84
E6	15.85	28.25	2.16	Na_2SiO_3	Si	82	38.28
E7	20.08	24.60	1.49	$Na_2Si_2O_5$	Na	74	37.39
E8	20.54	23.46	1.39	$Na_2Si_2O_5$	Na	77	37.73
E9	23.21	22.27	1.17	$Na_2Si_2O_5$	Na	79	37.95

Table 7
Level mean SNR of each design parameter at different levels.

Level	Level mean SNRs (dB)			
	$SNR_{(Ms)}$	$SNR_{(Temperature)}$	$SNR_{(Time)}$	$SNR_{(Water)}$
1	34.95	36.80	36.83	36.92
2	38.06	36.68	36.88	36.75
3	37.69	37.22	37.66	37.40
Max.	38.06	37.22	37.66	37.40
Min.	34.95	36.68	36.83	36.75
ΔSNR	3.11	0.54	0.83	0.65
Rank	1	4	2	3

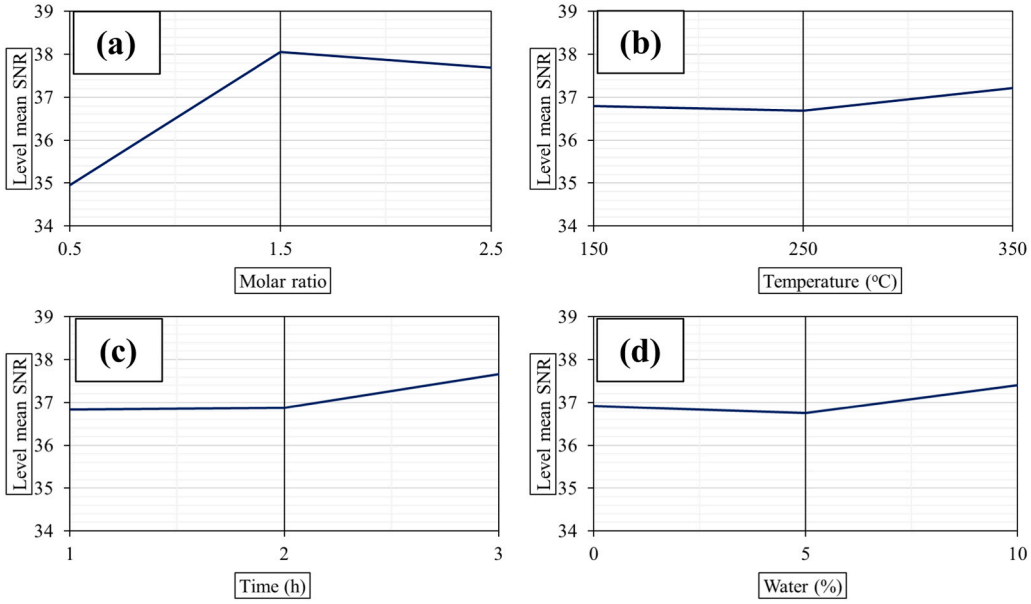

Fig. 5. Effect of design parameters (a) molar ratio, (b) temperature, (c) heating time, and (d) water dosage at different levels (Larger the better).

poorly structured silicates [56–58].

3.2. *Efficiency of the DA*

The quantitative efficiency was assessed via EDS-derived Na/Si molar ratios and stoichiometric assignment of silicate phases using Eqs. (4–7) and the results are given in Table 6. The results indicate progressive conversion from Si-rich trisilicate to Na-rich orthosilicate and finally to metasilicate phases. Sodium silicate yields varied from 53% to 82%, highlighting the strong influence of process

Table 8
Percentage contribution of each design parameter.

Parameter	DOF		Sum of squares		% Contribution (SS_k/SS_T) *100
	(*l*-1)	(*n*-1)	SS_k	SS_T	
Molar ratio	2	8	9.14	12.74	71.8
Temperature			0.38		3.0
Duration			2.07		16.3
Water			1.15		9.0

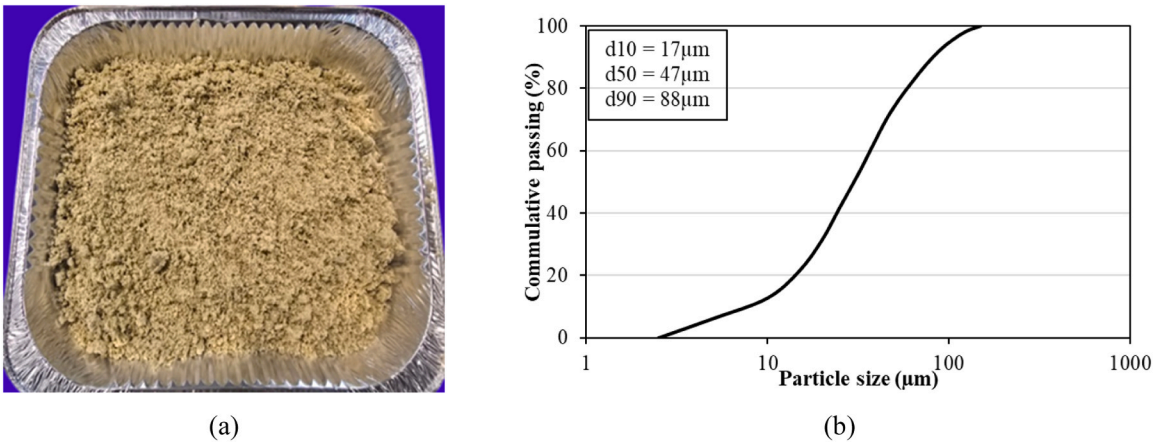

Fig. 6. Optimised DA (E4): (a) Visual appearance, (b) particle size distribution.

parameters. The maximum yield (82%) occurred for E6 (Ms = 1.5, 350 °C, 1 h, 5% water), consistent with balanced alkali–silica availability and enhanced ion diffusion. On the other hand, Na-rich E2 (Ms = 0.5, 250 °C) produced only 53% sodium silicate, dominated by low-polymerised Na_4SiO_4. Intermediate-to-high efficiencies were achieved for E5, E6, E7, E8, and E9, indicating the robustness of synthesis when Si and Na availability were well balanced and thermal activation remained within a 250–350°C window.

The theoretical energy required to heat 1 kg of silicate material from 25 °C to 350 °C can be calculated as: $Q = mc_p\Delta T$, where: C_p (glass) = 0.80–0.90 kJ/kg.K, and T = 325 K, thus: Q = 276 kJ/kg or 0.077kWh/kg [59]. Considering practical electric furnace efficiencies of 15–30% [60], the effective energy demand increases to approximately 0.35–0.6 kWh/kg. Similarly, the energy required for heating at 150 °C is estimated to be 0.1–0.2 kWh/kg, which is approximately three times lower than the energy demand for heating at 350 °C. Consequently, increasing activation temperature from 150 °C to 350 °C significantly increases energy consumption and associated CO_2 emissions, while improving sodium silicate formation efficiency by only 2%. The marginal performance gain does not justify the substantially higher thermal energy and carbon burden. Therefore, E4 represents a more sustainable optimisation balance. Furthermore, high-temperature activation can promote the formation of dense, less-reactive crystalline phases, whereas E4 preserves the amorphous nature of sodium metasilicate, which is more desirable for GP reactivity. The identified optimum corresponds to experiment E4 within the L_9 array; hence, the optimum performance is experimentally verified, and E4 was adopted as the optimum condition for making one-part GPCs.

3.3. Influence of design parameters on activator's efficiency

The mean SNRs of each design parameter at different levels, which represent the characteristic response of sodium-silicate formation, are presented in Table 7, while their variations are illustrated in Fig. 5. The maximum SNR value in each plot indicates the optimal level of the corresponding factor. Among all parameters, the SiO_2/Na_2O molar ratio exerted the greatest influence on sodium-silicate formation, showing the largest ΔSNR of 3.11 dB across its levels. Extremely low ratios resulted in Na-rich environments that promoted the formation of low-polymerised orthosilicate phases (Na_4SiO_4), whereas very high ratios provided insufficient alkalinity for activating the silica network. The optimum performance at level 2 (Ms = 1.5) reflects a balanced alkali–silica composition that facilitates the formation of reactive sodium-metasilicate species (Na_2SiO_3).

The reaction time was identified as the second most influential parameter (ΔSNR = 0.83 dB), indicating that sufficient holding time is necessary to complete the Na-Si coupling reaction and achieve maximum silicate conversion. Beyond this duration, further heating provides only minor improvement due to dehydration and phase densification. The water content ranked third (ΔSNR = 0.65 dB), suggesting a minor yet positive effect. Limited moisture (10 wt%) improved ionic diffusion and promoted homogeneous alkali distribution, thereby supporting the Na-Si interfacial reaction during low-temperature activation

The activation temperature showed smallest contribution (ΔSNR = 0.54 dB). A gradual increase in SNR with temperature

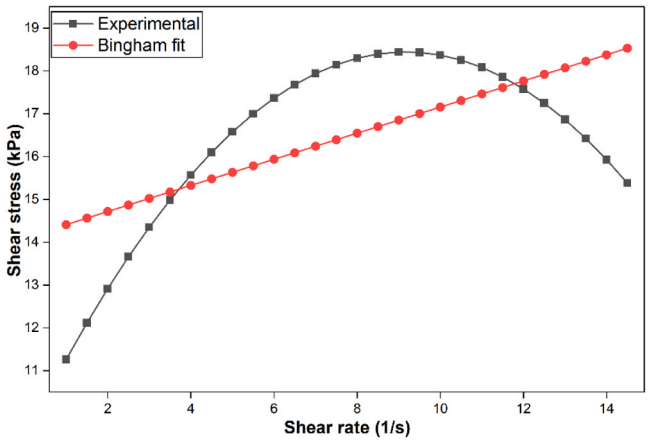

Fig. 7. Flow curve of GP paste made of WGP-derived activator using DA/b and w/b ratios of 0.4, and 0.35.

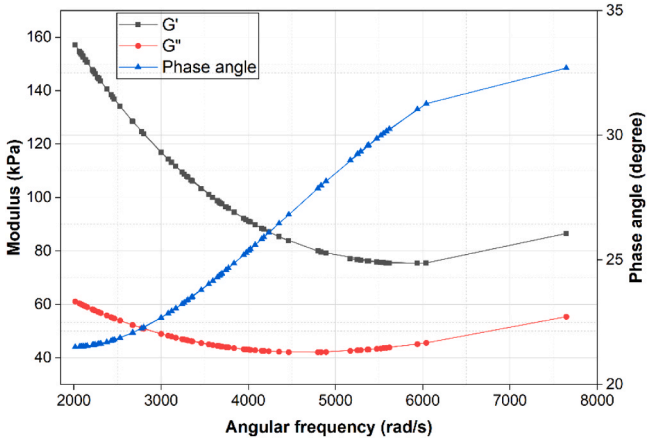

Fig. 8. Evaluation of the viscoelastic parameters as a function of angular frequency for one-part GP paste made using DA/b and w/b ratios of 0.4.

(150–350 °C) confirmed that higher thermal input enhances carbonate decomposition and silicate polymerisation; however, the improvement is modest compared with compositional effects. Therefore, a lower activation temperature of 150 °C, as used in the G4 mix, was considered the most practical and energy-efficient condition for achieving high reactivity without unnecessary power consumption or crystallisation of less-reactive phases.

The corresponding ANOVA results (Table 8) confirmed these findings, with the molar ratio contributing approximately 71.8% of the total variation in sodium-silicate yield, followed by reaction time (16.3%), water content (9%), and temperature (3%). Consequently, G4 (1.5 Ms, 150 °C, 2 h, 10% H_2O) was selected as the optimum synthesis condition, as it achieves near-maximum sodium-silicate yield under low-temperature and energy-efficient operation.

The qualitative trends observed in FTIR spectra aligned with the quantitative EDS-derived efficiencies. Activators showing sharp and distinct dual peaks in the 950–1050 cm^{-1} range (e.g., G4, G6) corresponded to high sodium silicate yields (80%), confirming the presence of well-structured Si–O–Na linkages. Samples with broader, underdeveloped bands (e.g., G1, G9) matched lower yields, verifying that poorly balanced alkali/silica ratios hinder the formation of polymerised sodium silicate networks. The optimised sample (E4) yielded a homogeneous, fine powder (true density of 2.14 g/cm^3 in comparison to 2.31 g/cm^3 for FA) suitable for direct use in one-part GP composites (Fig. 6).

3.4. Evaluation of one-part geopolymer composites

3.4.1. Rheological behaviour of one-part geopolymer composites

The flow curve (Fig. 7), obtained through a controlled shear rate sweep, revealed a clear yield-pseudoplastic behaviour. The paste initially resisted flow, displaying a yield plateau, followed by a nonlinear increase in shear stress with shear rate, characteristic of a Bingham fluid with mild shear-thinning.

Using linear regression, the Bingham model fit yielded a yield stress of 14.106 kPa and a plastic viscosity of 305.08 Pa·s. These values reflect a highly cohesive matrix with strong internal structure formed from early GP gelation. Such behaviour is beneficial for

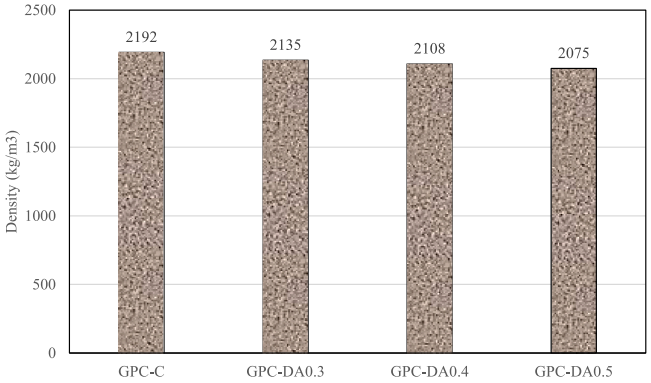

Fig. 9. Density of one-part GPCs varying the DA to binder ratio.

shape retention, reduced segregation, and enhanced buildability during placement. The Herschel-Bulkley model was initially evaluated to capture potential non-linear shear-thinning behaviour. However, the experimental flow curve exhibits a peak shear stress followed by a reduction at higher shear rates, indicating structural breakdown and thixotropic behaviour. Since the Herschel-Bulkley model assumes monotonic stress increase with shear rate, it does not adequately represent this behaviour. Consequently, the Bingham approximation was retained for engineering interpretation, while acknowledging the thixotropic nature of the geopolymer paste. The relatively low coefficient of regression ($R^2 = 0.35$) obtained from the Bingham model indicates deviation from ideal linear plastic behaviour. This deviation suggests that the GP paste exhibits non-linear shear-thinning characteristics and structural breakdown under increasing shear rates, which are typical of alkali-activated and cementitious systems. The Bingham approximation was retained in this study to enable straightforward comparison with conventional cementitious materials and to provide engineering-relevant parameters for practical casting applications. The observed deviation does not invalidate the rheological interpretation but rather reflects the complex thixotropic and shear-dependent nature of the dry-activated GP matrix.

Fig. 8 presents the storage modulus (G'), loss modulus (G''), and phase angle (δ) as functions of angular frequency for the WGP-based one-part GP paste. The data provide a comprehensive view of the material's viscoelastic behaviour and phase response under dynamic loading.

The storage modulus (G'), representing the elastic (recoverable) component, consistently exceeded the loss modulus (G'') across the entire frequency range. This dominance of G' over G'' confirms a solid-like, gelled structure typical of early Geo-P. Both moduli first decreased and then increased with frequency, indicative of shear stiffening, as the internal network becomes more resistant to deformation under higher oscillation rates.

Importantly, the phase angle increased progressively with frequency, reaching values above 35° at high frequencies. This trend suggests a gradual increase in the viscous contribution (G'') relative to the elastic response (G'), particularly under rapid deformations. While the system remains in the elastic-dominant regime (as $G' > G''$), this rising phase angle indicates that energy dissipation becomes more pronounced at higher frequencies, potentially due to microstructural reorientation or limited mobility of unreacted species within the partially gelled network.

The stiffening moduli with a rising phase angle are favourable for applications that require a balance between shape retention and deformation resistance, such as extrusion-based additive manufacturing, where moderate flow under pressure and solid-like recovery after deposition are crucial. From a practical construction perspective, the observed rheological behaviour has important implications for casting and placement. The measured yield stress indicates that the paste possesses sufficient structural build-up to resist segregation and bleeding under static conditions, which is beneficial for mould filling and dimensional stability. At the same time, the shear-thinning behaviour implies that viscosity decreases under applied shear during mixing, pumping, or vibration, facilitating workable placement without excessive compaction energy. The dominance of storage modulus ($G' > G''$) suggests a stable, elastic-dominant network capable of retaining shape after placement, which is advantageous for both conventional casting and extrusion-based additive manufacturing applications. Collectively, these rheological characteristics indicate that the optimised dry-activated geopolymer paste exhibits a balance between flowability under shear and structural stability at rest, making it suitable for practical construction scenarios.

3.4.2. Physical and mechanical properties of one-part geopolymer composites

3.4.2.1. Hardened Density. The measured densities of the GPC mixes are presented in Fig. 9. The conventional two-part GPC (GPC-C) exhibited the highest density of 2192 kg/m^3, consistent with prior studies using liquid sodium silicate and sodium hydroxide solutions [61,62]. While the one-part mixes incorporating WGP-based DA (GPC-DA0.3 to GPC-DA0.5) showed progressively lower densities, ranging from 2135 to 2075 kg/m^3. This gradual reduction in density with increasing DA content can be attributed to the lower specific gravity of the DA compared to the liquid alkali solutions, as well as the higher entrapped porosity during mixing due to the powder form. Additionally, as the DA-to-binder ratio increased, more low-density DA (2.14 g/cc) replaced a portion of the higher-density FA (2.31 g/cc), further contributing to the decrease. Despite this reduction, the densities of DA-based GPC remained well within the

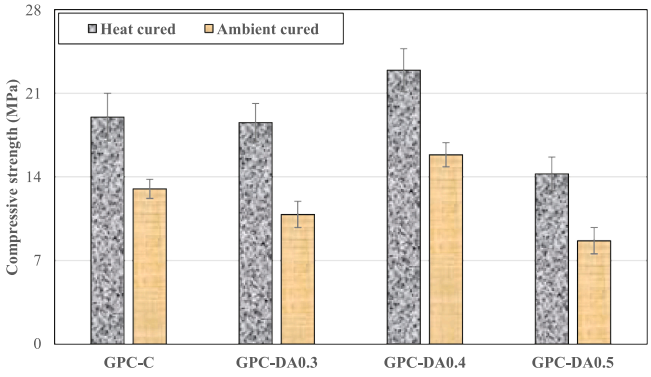

Fig. 10. Compressive strength of WGP-derived DA-based one-part GPC.

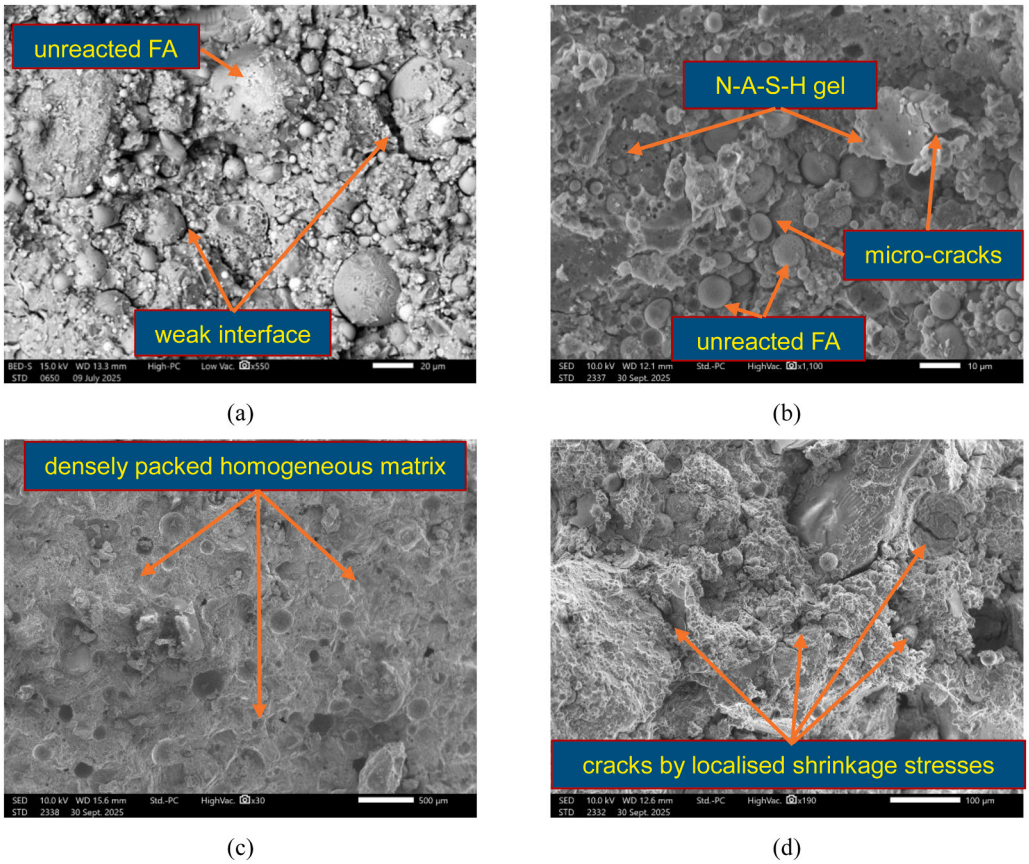

Fig. 11. SEM images of one-part GPCs (a) GPC-C, (b) GPC-0.3DA, (c) GPC-0.4DA, and (d) GPC-0.5DA.

acceptable range (2000–2230 kg/m^3) for structural concrete applications [63], indicating that lightweighting benefits can be achieved without compromising the mix's integrity.

3.4.2.2. Compressive strength. Fig. 10 presents the compressive strength development of GPC mixes under ambient and heat curing (60°C) conditions. As expected, all mixes exhibited superior performance under heat curing due to the accelerated geo-polymerisation kinetics at elevated temperatures. Notably, the DA-based mix (GPC-DA0.4) consistently outperformed the conventional GPC mix (GPC-C) regardless of curing conditions. Under heat curing, the strength increased from 19 ± 2 MPa for GPC-C to 22.93 ± 1.8 MPa for GPC-DA0.4, representing a 20.7% improvement. Similarly, under ambient conditions, strength rose from 13 ± 0.8 MPa (GPC-C) to 15.85 ± 1 MPa (DA-GPC0.4), marking a 22% enhancement.

This trend may seem peculiar, given that GPC-C incorporated commercial liquid sodium silicate, which is traditionally considered

more reactive. However, several factors contribute to the superior performance of DA mixes. Firstly, the commercial sodium silicate solution used in GPC-C contains a significant proportion of water (about 50%), which increases the water-to-binder ratio, dilutes the activator, and results in higher porosity and reduced gel densification. In contrast, DA mixes allow better control over water content and facilitate in-situ formation of sodium silicate via the thermochemical reaction between sodium hydroxide and the silica-rich WGP. This yields a more intimately bonded, highly cross-linked aluminosilicate gel network. Moreover, the dry blending process ensures more uniform activator dispersion, eliminating the segregation and alkali leaching risks typically associated with liquid activators. The inclusion of WGP also contributes additional pozzolanic reactivity and a micro-filler effect, further enhancing matrix densification. Collectively, these mechanisms explain the observed strength gains in DA-GPC mixes, particularly at higher activator dosages.

The mix GPC-DA0.5 exhibited a noticeable decline in compressive strength compared to GPC-DA0.4, with values reducing to 14.25 $\pm$ 1.4 MPa (heat-cured) and 8.65 $\pm$ 1.1 MPa (ambient-cured). This reduction indicates that further increase in the DA dosage beyond the optimum leads to over-alkalisation of the matrix. Excessive Na_2O promotes rapid precipitation of aluminosilicate gel, generating localised shrinkage stresses and microcracks during curing. Consequently, the microstructure becomes more porous and brittle, resulting in premature load failure. Overall, GPC-DA0.5 demonstrates the threshold of activator efficiency, where additional alkali no longer contributes to strength development and instead destabilises the GP network, confirming GPC-DA0.4 as the optimum mix for mechanical and structural stability. These findings underscore the effectiveness of thermochemically synthesised DAs in delivering comparable or even superior performance to traditional liquid-based systems.

3.4.3. Microstructural analysis of the produced geopolymer composite

3.4.3.1. SEM. Fig. 11 shows the SEM micrographs of GPCs made using conventional liquid activators (GPC-C) and DA-based systems by varying DA/binder ratios. The comparative analysis highlights the distinct microstructural evolution with increasing DA dosage and represents the effectiveness of the thermochemically synthesised WGP-based activators.

The control GPC-C (Fig. 11a), produced with commercial sodium silicate and sodium hydroxide solutions, reveals a loosely packed and heterogeneous matrix. Several unreacted FA particles are visible, surrounded by insufficiently polymerised binder phases. The weak interface and porous nature of the matrix indicate that the rapid reaction and poor workability of liquid activator systems may hinder complete precursor dissolution and homogenous gel formation. In contrast, the GPC-DA0.3 sample (Fig. 11b) exhibits slight improvements but still retains notable unreacted FA particles and microcracks, indicating limited alkali activation due to an insufficient activator dosage. The matrix remains porous and disjointed, leading to poor structural integrity and reduced compressive strength. A more refined microstructure is observed in GPC-DA0.4 (Fig. 11c), with the appearance of well-distributed N–A–S–H gel phases, exhibits a densely packed, homogeneous matrix with minimal porosity and strong binder cohesion. A continuous gel network is evident, and only a few glass residues are observed, likely acting as inert micro-fillers. The superior microstructure corresponds with the highest compressive strength observed across all mixes, confirming that higher DA content promotes better geo-polymerisation and microstructural development. This aligns with improved mechanical and rheological performance recorded for this mix.

The GPC-DA0.5 mix (Fig. 11d) shows a porous and partially compacted matrix with visible microcracks and unreacted particles, indicating over-activation. Excess alkali led to rapid gel precipitation and localized shrinkage, producing an inhomogeneous and brittle structure. Although chemically well-activated, the discontinuous N–A–S–H gel and weak particle bonding reduced compressive strength compared to the denser, more uniform matrix observed in GPC-DA0.4. The SEM observations presented in this study are primarily qualitative and intended to support the trends observed in mechanical performance. Quantitative image analysis, such as porosity estimation, pore size distribution, or gel area fraction measurement, was not conducted. While the micrographs provide visual confirmation of matrix densification and gel formation, future work incorporating quantitative image processing techniques would enable more rigorous correlation between microstructure and mechanical behaviour.

4. Sustainability and circular economy analysis

4.1. Methodology

A comparative cost and CO_2 emission analysis was carried out for all GP mixes investigated in this study (conventional GPC, DA-based GPCs) and for a baseline OPC concrete. The calculations were normalised to 1 m^3 of mortar/composite. Each mix was designed with the mix proportions used in this study, shown in Table 4. The OPC baseline assumed the sand volume (0.6 m^3) and a 0.4 m^3 cement paste volume, using a typical cement density of 3150 kg/m^3. The analysis followed an A1-A3 (cradle-to-gate) life-cycle boundary, accounting for raw material production, processing, and transportation while excluding operational aspects such as energy consumption during curing, maintenance, service life performance, and end-of-life disposal or recycling to simplify the analysis.

4.2. Input parameters

The emission factors and unit costs were primarily drawn from Australian LCA studies, standard inventory sources, the Australian AusLCI database, and environmental product declarations. The embodied CO_2e for OPC is estimated to be 0.7–0.9 kg CO_2e/kg, and the cost is 0.25 AUD/kg, consistent with local life-cycle studies [64,65]. FA has emissions (0.02 kg CO_2e/kg) based on industry fact sheets, and its average cost is 0.06–0.10 AUD/kg in Queensland markets [66]. Industrial activators like sodium hydroxide and sodium silicate, known for high embodied energy, carry emissions and cost of 0.7–1.12 kg CO_2e/kg, 0.90 AUD/kg, and 0.5–0.7 kg CO_2e/kg, 1.1

Table 9
Input values for cost and CO_2 analysis.

Material	FA	WGP	Sand	NaOH	Na_2SiO_3	OPC
Unit Cost (AUD/kg)	0.08	0	0.1	0.9	1.1	0.25
Emission (kg CO_2e/kg)	0.02	0	0.005	1.12	0.7	0.85

AUD/kg, respectively [67,68]. Fine sand emissions are modest (0.0048 kg CO_2e/kg), with cost estimates of around 0.08 AUD/kg, based on Australian national price indices [69]. WGP was treated as waste materials, following ISO 14044 cut-off allocation; no embodied cost or CO_2e was assigned to them. The alternative allocation for WGP (e.g., economic allocation including processing) may alter absolute values. Distances were assigned as 50 km for OPC, FA, sand, and activators, 50 km for WGP. The selected values are given in Table 9.

The transport distances and emission factors adopted in this study represent scenario-specific assumptions based on regional supply chain conditions and publicly available databases. These values may vary depending on geographical location, material sourcing practices, and transportation logistics. Therefore, the absolute embodied CO_2 and cost values reported here should be interpreted within the defined system boundary and regional context. However, the comparative trends between conventional and dry activated systems are expected to remain consistent, as the dominant contribution arises from activator production rather than transport.

4.3. Calculations

For each mix, the total cost and embodied CO_2 emissions were calculated using Eqs. 13 and 14, and the results are given in Table 10 and Fig. 12.

$$C_T\left(AUD/m^3\right) = \sum_i (m_i.c_i) + \sum_i \left(\frac{m_i}{1000} \cdot d_i.f_{trans-cost}\right) \tag{13}$$

$$E_T\left(kg/m^3\right) = \sum_i (m_i.EF_i) + \sum_i \left(\frac{m_i}{1000} \cdot d_i.f_{trans-CO2}\right) \tag{14}$$

Where m_i = mass of material i (kg/m^3), c_i = unit cost (AUD/kg), EF_i = unit CO_2 emissions (kg/kg), d_i = transport distance (km), $f_{trans-cost}$ = 0.14 AUD/t.km, and $f_{trans-CO2}$ = 0.102 CO_2/t.km (Australian road freight).

The OPC mix recorded the highest embodied CO_2 emissions (1031 kg/m^3) and a total cost of 463 AUD/m^3, driven by the high clinker content in OPC and its associated production and transport emissions. In comparison, the conventional GPC-C mix, while emitting only 404 kg/m^3 of CO_2e, was the most expensive at 704 AUD/m^3, primarily due to the high cost of commercial sodium silicate and sodium hydroxide.

In contrast, the DA-based mixes (DA0.3–DA0.5) achieved significant reductions in both environmental and economic metrics. The GPC-DA0.3 mix demonstrated the lowest total CO_2e (129 kg/m^3) and cost (301 AUD/m^3), representing an 68% reduction in CO_2 emissions and a 57% cost savings compared to GPC-C. Even at higher DA dosages (GPC-DA0.5), the CO_2 emissions and cost remained significantly lower than both OPC and GPC-C, at 189 kg/m^3 and 352 AUD/m^3, respectively. The key contributor to these improvements is the replacement of energy and emission-intensive commercial sodium silicate with thermochemically synthesised sodium silicate derived from WGP. This valorisation of waste not only reduces material cost and embodied emissions to near zero but also minimises transport-related impacts due to the local availability of waste-based activators. The contributions of each parameter towards the total CO_2 emissions and material cost in making one-part GPCs using WGP-based DA are shown in Fig. 13. The OPC system is highly dominated by cement production, which accounts for 68% of total cost and 98% of total embodied CO_2, confirming the high environmental burden of clinker manufacturing. In contrast, the GP mixes distribute their impacts more evenly among raw materials. For the GPC-C mix, sodium silicate and sodium hydroxide together contribute nearly 70% of total cost and 90% of total CO_2, reflecting the high energy demand of industrial activators. Substituting these with waste-derived DAs (DA0.3–DA0.5) substantially reduces both cost and emissions by up to 55–70% compared with GPC-C as FA and sand become the main contributors (40–60% of cost) with very low embodied CO_2. In the DA-based systems, sodium hydroxide remains the largest single contributor to CO_2 (70–80%), while transport represents only 5–8% of total impacts across all mixes. Overall, the analysis confirms that replacing commercial activators with dry-processed waste-derived alternatives significantly improves both the economic and environmental performance of GP binders.

5. Conclusions

This study successfully developed a sustainable and cost-effective one-part GP binder system by synthesising solid alkaline activators from silica-rich waste glass powder through a thermochemical method. The following key conclusions can be drawn:

- Waste glass powder can be synthesised to sodium silicate rich dry activators via a thermochemical process, confirmed by EDS and FTIR through the presence of sodium silicate phases. This validates waste glass as a viable silica source for producing reactive and sustainable solid activators.

Table 10
Comparison of cost and embodied CO_2 emissions of OPC and DA-based GP mixes.

Mix type	Material* Cost (AUD/m^3)	Transport Cost (AUD/m^3)	Total Cost (AUD/m^3)	Materials* CO_2e (kg/m^3)	Transport CO_2e (kg/m^3)	Total CO_2e (kg/m^3)
OPCC	442.20	19.95	462.15	1015.63	14.54	1030.17
GPC-C	682.63	20.84	703.47	388.51	15.19	403.7
GPC-DA0.3	280.67	19.55	300.22	114.43	14.24	128.68
GPC-DA0.4	307.13	18.61	325.74	143.83	13.57	157.40
GPC-DA0.5	333.68	20.84	352.52	173.33	15.21	188.54

Note: * = Include OPC, FA, WGP, sodium hydroxide, and sodium silicate.

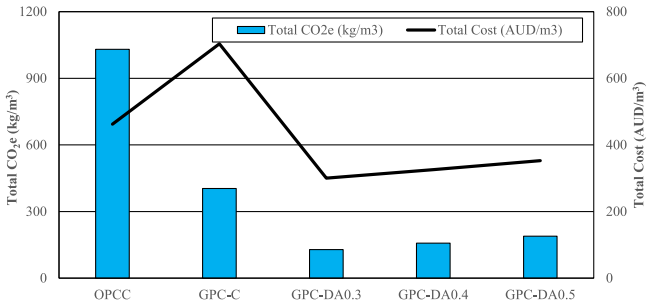

Fig. 12. CO_2 emissions and cost of producing one cubic meter of one-part GPCs.

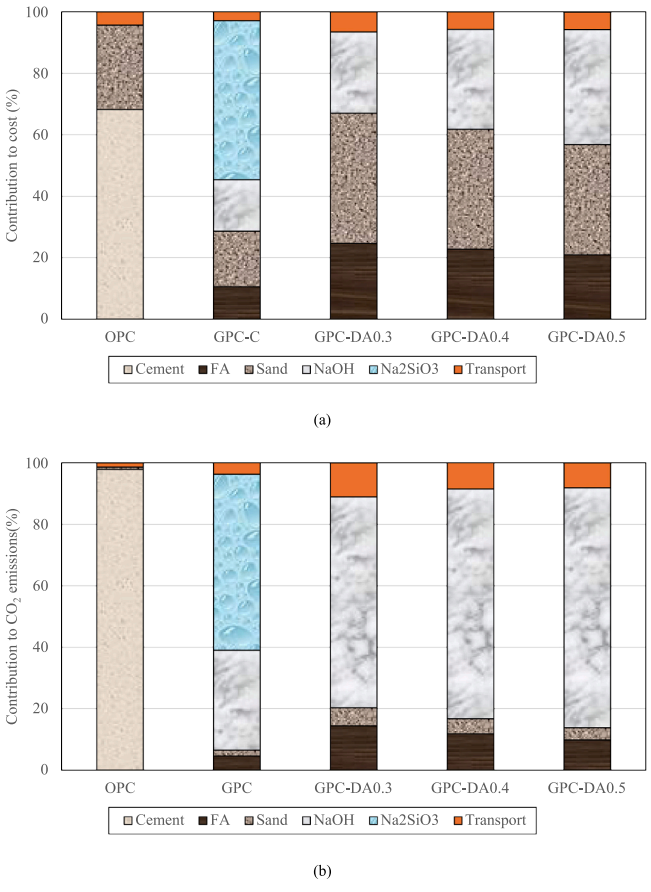

Fig. 13. Contribution of individual constituents to (a) cost (AUD/m^3) and (b) embodied CO_2 emissions (kg/m^3) for OPC, GPC, GPC–DA0.3, and GPC-DA0.5 mixes.

- The silica-to-sodium oxide molar ratio had the greatest effect on sodium silicate yield (72%), followed by reaction time (16%), water addition (9%), and temperature (3%). The optimum condition 1.5 ratio, 150 °C, 2 h, and 10 wt% water produced a balanced alkali-silica environment and up to 80% sodium silicate yield.
- The Taguchi SNR-ANOVA method effectively predicted and optimised activator yield with minimal trials, confirming its reliability for designing efficient thermochemical synthesis processes.
- Fresh GPC pastes with dry activator (DA/binder = 0.4) revealed a shear-thinning, Bingham-type flow. Oscillatory testing indicated increasing storage and loss moduli with angular frequency and a moderate rise in phase angle, signifying an elastic-dominant yet dissipative matrix may be ideal for field placement and 3D printing.
- GPC-DA0.4 mix achieved superior compressive strength (up to 24.5 MPa under heat curing) compared to the control liquid-activated GPC (18.5 MPa). This is attributed to better activator dispersion, in-situ sodium silicate formation, and matrix densification via the pozzolanic and micro-filler effects of waste glass.

- The one-part GPC mixes showed a 3–5% lower density than conventional GPC due to the lighter activator with maintained structural integrity. SEM micrographs validated a more compact and less porous matrix in DA mixes at higher activator dosages.
- Incorporating dry activators derived from waste glass significantly reduced environmental and economic burdens. At optimal dosages, the DA-based mix achieved a 60% reduction in CO_2 emissions and 54% cost savings compared to conventional GPC, and up to 85% lower CO_2 footprint compared to OPC concrete.

This work provides a practical alternative to conventional GPCs by introducing a safe, dry, and waste-derived activator system, suitable for field use, low-carbon construction. In this study, compressive strength was used as the primary mechanical indicator to evaluate the effectiveness of the thermochemically synthesised dry activator at the material screening stage. While the results demonstrate promising performance relative to conventional activator systems, additional properties such as flexural strength, tensile splitting strength, shrinkage behaviour, long-term durability, and chemical resistance should be evaluated in future investigations to fully establish structural suitability of the developed one-part geopolymer system. The sustainability assessment is limited to material production and transport stages; curing energy and long-term service performance were not included and deserve further investigation in future studies. Future work will also explore activator synthesis from other agro-industrial waste sources like ceramic waste powder, sugarcane bagasse ash.

CRediT authorship contribution statement

Seemab Tayyab: Writing – original draft, Validation, Methodology, Investigation, Formal analysis, Data curation, Conceptualization. **Wahid Ferdous:** Writing – review & editing, Supervision, Resources, Project administration, Methodology, Conceptualization. **Weena Lokuge:** Writing – review & editing, Supervision, Resources. **Tuan Ngo:** Writing – review & editing. **Andreas Gerdes:** Writing – review & editing. **Allan Manalo:** Writing – review & editing, Supervision.

Declaration of Competing Interest

The authors declare that they have no known competing financial interests or personal relationships that could have appeared to influence the work reported in this paper.

Acknowledgment

The first author acknowledges the financial support he received from the University of Southern Queensland, Australia, through the UniSQ International Stipend and International Fees Research Scholarship for the purpose of carrying out his PhD studies. The authors also acknowledge the support from the Queensland-Germany Bioeconomy Collaborative Science Program (QLDBMBF 23018) to the project “Net-zero carbon cement from biomass wastes”.

Data availability

Data will be made available on request.

References

[1] M. Amran, N. Makul, R. Fediuk, Y.H. Lee, N.I. Vatin, Y.Y. Lee, K. Mohammed, Global carbon recoverability experiences from the cement industry, Case Stud. Constr. Mater. 17 (2022) e01439, https://doi.org/10.1016/J.CSCM.2022.E01439.
[2] J.L. Provis, Alkali-activated materials, Cem. Concr. Res. 114 (2018) 40–48, https://doi.org/10.1016/J.CEMCONRES.2017.02.009.
[3] T. Srividya, P.R. Kannan Rajkumar, M. Sivasakthi, A. Sujitha, R. Jeyalakshmi, A state-of-the-art on development of geopolymer concrete and its field applications, Case Stud. Constr. Mater. 16 (2022) e00812, https://doi.org/10.1016/J.CSCM.2021.E00812.
[4] J. Zhang, C. Shi, Z. Zhang, Z. Ou, Durability of alkali-activated materials in aggressive environments: a review on recent studies, Constr. Build. Mater. 152 (2017) 598–613, https://doi.org/10.1016/J.CONBUILDMAT.2017.07.027.
[5] J. Zhang, C. Shi, Z. Zhang, Z. Ou, Durability of alkali-activated materials in aggressive environments: a review on recent studies, Constr. Build. Mater. 152 (2017) 598–613, https://doi.org/10.1016/J.CONBUILDMAT.2017.07.027.
[6] Y. Fu, L. Cai, W. Yonggen, Freeze–thaw cycle test and damage mechanics models of alkali-activated slag concrete, Constr. Build. Mater. 25 (2011) 3144–3148, https://doi.org/10.1016/J.CONBUILDMAT.2010.12.006.
[7] S.K. Rahman, R. Al-Ameri, Marine geopolymer concrete—a hybrid curable self-compacting sustainable concrete for marine applications, Appl. Sci. 12 (2022), https://doi.org/10.3390/app12063116.
[8] A. Ahmad, A. Alsaid, P.D. Student, Rev. Prop. Perform. Appl. Geopolym. Concr. 2 (2019) 61–75, https://doi.org/10.26392/SSM.2019.02.01.061.
[9] H. Zhong, M. Zhang, 3D printing geopolymers: a review, Cem. Concr. Compos 128 (2022) 104455, https://doi.org/10.1016/J.CEMCONCOMP.2022.104455.
[10] T. Luukkonen, Z. Abdollahnejad, J. Yliniemi, P. Kinnunen, M. Illikainen, One-part alkali-activated materials: a review, Cem. Concr. Res. 103 (2018) 21–34, https://doi.org/10.1016/J.CEMCONRES.2017.10.001.
[11] A. Kallamalayil Nassar, P. Kathirvel, Effective utilization of agricultural waste in synthesizing activator for sustainable geopolymer technology, Constr. Build. Mater. 362 (2023) 129681, https://doi.org/10.1016/J.CONBUILDMAT.2022.129681.
[12] L.K. Turner, F.G. Collins, Carbon dioxide equivalent (CO2-e) emissions: a comparison between geopolymer and OPC cement concrete, Constr. Build. Mater. 43 (2013) 125–130, https://doi.org/10.1016/J.CONBUILDMAT.2013.01.023.
[13] M.F. Alnahhal, A. Hamdan, A. Hajimohammadi, T. Kim, Effect of rice husk ash-derived activator on the structural build-up of alkali activated materials, Cem. Concr. Res. 150 (2021) 106590, https://doi.org/10.1016/J.CEMCONRES.2021.106590.
[14] F.A. Shilar, S.V. Ganachari, V.B. Patil, T.M.Y. Khan, S. Dawood Abdul Khadar, Molarity activity effect on mechanical and microstructure properties of geopolymer concrete: a review, Case Stud. Constr. Mater. 16 (2022) e01014, https://doi.org/10.1016/J.CSCM.2022.E01014.

[15] A.İ. Çelik, U. Tunç, A. Bahrami, M. Karalar, M.A. Othuman Mydin, T. Alomayri, Y.O. Özkılıç, Use of waste glass powder toward more sustainable geopolymer concrete, J. Mater. Res. Technol. 24 (2023) 8533–8546, https://doi.org/10.1016/J.JMRT.2023.05.094.
[16] R. Vinai, M. Soutsos, Production of sodium silicate powder from waste glass cullet for alkali activation of alternative binders, Cem. Concr. Res. 116 (2019) 45–56, https://doi.org/10.1016/J.CEMCONRES.2018.11.008.
[17] S. Ouyang, W. Chen, Z. Zhang, X. Li, W. Zhu, Experimental study of one-part geopolymer using different alkali sources, J. Phys. Conf. Ser. 1605 (2020) 12155, https://doi.org/10.1088/1742-6596/1605/1/012155.
[18] N. Ye, J. Yang, S. Liang, Y. Hu, J. Hu, B. Xiao, Q. Huang, Synthesis and strength optimization of one-part geopolymer based on red mud, Constr. Build. Mater. 111 (2016) 317–325, https://doi.org/10.1016/J.CONBUILDMAT.2016.02.099.
[19] K. Yin, Y. Jiang, H. He, J. Ren, Z. Li, Characterization of one-part alkali-activated slag with rice straw ash, Constr. Build. Mater. 345 (2022) 128403, https://doi.org/10.1016/J.CONBUILDMAT.2022.128403.
[20] Q. Zhao, C. Ma, B. Huang, X. Lu, Development of alkali activated cementitious material from sewage sludge ash: two-part and one-part geopolymer, J. Clean. Prod. 384 (2023) 135547, https://doi.org/10.1016/J.JCLEPRO.2022.135547.
[21] R.A.M. Figueiredo, P.R.G. Brandão, M. Soutsos, A.B. Henriques, A. Fourie, D.B. Mazzinghy, Producing sodium silicate powder from iron ore tailings for use as an activator in one-part geopolymer binders, Mater. Lett. 288 (2021) 129333, https://doi.org/10.1016/J.MATLET.2021.129333.
[22] M.H. Samarakoon, P.G. Ranjith, W.H. Duan, V.R.S. De Silva, Properties of one-part fly ash/slag-based binders activated by thermally-treated waste glass/NaOH blends: a comparative study, Cem. Concr. Compos 112 (2020) 103679, https://doi.org/10.1016/J.CEMCONCOMP.2020.103679.
[23] Y.O. Özkılıç, M. Karalar, A.İ. Çelik, M.R. Alasiri, M.A. Mohamud, Microstructural, mechanical and statistical evaluation of concrete incorporating waste glass wool exposed to elevated temperatures, Sci. Rep. 16 (2025) 434, https://doi.org/10.1038/s41598-025-29957-5.
[24] C. Aksoylu, B. Başaran, M. Karalar, Ö. Zeybek, E. Althaqafi, A.N. Beskopylny, S.A. Stel'makh, E.M. Shcherban', O.A. Umiye, Y.O. Özkılıç, Experimental, theoretical and digital image correlation methods to assess bending performance of RC beams with recycled glass powder replacing cement, Sci. Rep. 15 (2025) 25163, https://doi.org/10.1038/s41598-025-08710-y.
[25] C. Shi, Y. Wu, C. Riefler, H. Wang, Characteristics and pozzolanic reactivity of glass powders, Cem. Concr. Res. 35 (2005) 987–993, https://doi.org/10.1016/j.cemconres.2004.05.015.
[26] A. Siddika, A. Hajimohammadi, Md.A.Al Mamun, R. Alyousef, W. Ferdous, Waste glass in cement and geopolymer concretes: a review on durability and challenges, Polymers 13 (2021), https://doi.org/10.3390/polym13132071.
[27] R.J. Singh, A. Raut, A.L. Murmu, M. Jameel, Influence of glass powder incorporated foamed geopolymer blocks on thermal and energy analysis of building envelope, J. Build. Eng. 43 (2021) 102520, https://doi.org/10.1016/j.jobe.2021.102520.
[28] M. Torres-Carrasco, F. Puertas, Waste glass in the geopolymer preparation. Mechanical and microstructural characterisation, J. Clean. Prod. 90 (2015) 397–408, https://doi.org/10.1016/J.JCLEPRO.2014.11.074.
[29] A. Siddika, A. Hajimohammadi, W. Ferdous, V. Sahajwalla, Roles of waste glass and the effect of process parameters on the properties of sustainable cement and geopolymer concrete—a state-of-the-art review, Polymers 13 (2021), https://doi.org/10.3390/polym13223935.
[30] S. Janga, A.N. Raut, S.K. Das, Influence of static and cyclic thermal loadings on the performance of fly ash–steel slag and fly ash–glass powder-based geopolymer composites, J. Therm. Anal. Calor. 150 (2025) 10803–10820, https://doi.org/10.1007/s10973-025-14474-4.
[31] A.N. Raut, A.L. Murmu, S.C. Sapkota, S. Das, P. Saha, Experimental and machine learning-based analysis of oxide ratios in alumina-silicate geopolymer formation, Iran. J. Sci. Technol. Trans. Civ. Eng. (2025), https://doi.org/10.1007/s40996-025-01875-6.
[32] A. Subcommittee, ASTM C618-19," Standard Specification for Coal Fly Ash and Raw or Calcined Natural Pozzolan for Use in Concrete., (2019).
[33] P. Delgado-Plana, S. Bueno-Rodríguez, L. Pérez-Villarejo, D. Eliche-Quesada, Synthesis of solid sodium silicate from waste glass and utilization on one-part alkali-activated materials based on spent oil filtering earth, Environ. Sci. Pollut. Res. (2024), https://doi.org/10.1007/s11356-024-33368-w.
[34] E. Febriana, W. Mayangsari, S.D. Yudanto, E. Sulistiyono, M. Handayani, F. Firdiyono, A. Maksum, A.B. Prasetyo, J.W. Soedarsono, Novel method for minimizing reactant in the synthesis of sodium silicate solution from mixed-phase quartz-amorphous SIO2, Case Stud. Chem. Environ. Eng. 9 (2024) 100656, https://doi.org/10.1016/J.CSCEE.2024.100656.
[35] G. Taguchi, Taguchi Methods. Des. Exp. (No Title) (1993).
[36] Z. Shi, C. Shi, S. Wan, Z. Zhang, Effects of alkali dosage and silicate modulus on alkali-silica reaction in alkali-activated slag mortars, Cem. Concr. Res. 111 (2018) 104–115, https://doi.org/10.1016/J.CEMCONRES.2018.06.005.
[37] Z. Xu, J. Yue, G. Pang, R. Li, P. Zhang, S. Xu, Influence of the activator concentration and solid/liquid ratio on the strength and shrinkage characteristics of alkali-activated slag geopolymer pastes, Adv. Civ. Eng. 2021 (2021) 6631316, https://doi.org/10.1155/2021/6631316.
[38] H. Cheng, K.-L. Lin, R. Cui, C.-L. Hwang, Y.-M. Chang, T.-W. Cheng, The effects of SiO2/Na2O molar ratio on the characteristics of alkali-activated waste catalyst–metakaolin based geopolymers, Constr. Build. Mater. 95 (2015) 710–720.
[39] A.K. Nassar, P. Kathirvel, G. Murali, T. AlQemlas, M. Azab, Innovative one-part Alkali activated binder from activator derived from agricultural waste: synthesis and application for sustainable construction, Results Eng. 21 (2024) 101975.
[40] R. Sathish Kumar, K. Sureshkumar, R. Velraj, Optimization of biodiesel production from Manilkara zapota (L.) seed oil using Taguchi method, Fuel 140 (2015) 90–96, https://doi.org/10.1016/J.FUEL.2014.09.103.
[41] W. Ferdous, A. Manalo, T. Aravinthan, Bond behaviour of composite sandwich panel and epoxy polymer matrix: Taguchi design of experiments and theoretical predictions, Constr. Build. Mater. 145 (2017) 76–87, https://doi.org/10.1016/J.CONBUILDMAT.2017.03.244.
[42] M. Olivia, H. Nikraz, Properties of fly ash geopolymer concrete designed by Taguchi method, Mater. & Des. 36 (2012) 191–198, https://doi.org/10.1016/J.MATDES.2011.10.036.
[43] A.K. Nassar, P. Kathirvel, G. Murali, T. AlQemlas, M. Azab, Innovative one-part Alkali activated binder from activator derived from agricultural waste: synthesis and application for sustainable construction, Results Eng. 21 (2024) 101975, https://doi.org/10.1016/J.RINENG.2024.101975.
[44] S. Wu, M. He, M. Yang, B. Peng, Near-infrared spectroscopic study of OH stretching modes in Kaolinite and Dickite, Crystals 12 (2022), https://doi.org/10.3390/cryst12070907.
[45] H.Z. Cao, Y. Yao, G. Halada, H.J. Jung, T. Kim, Impact of naoh concentration on deweaving of cotton fabric in aqueous solutions, Sustain. (Switz.) 13 (2021) 1–10, https://doi.org/10.3390/su13042015.
[46] M. Shamsuyeva, Spectroscopy of PVC-based blends, IPNs, and gels, Poly(Vinyl Chloride)-Based Blends, Interpenetr. Polym. Netw. (IPNs) Gels (2024) 359–376, https://doi.org/10.1016/B978-0-323-99474-3.00021-5.
[47] H. Wang, H. Wu, Z. Xing, R. Wang, S. Dai, The effect of various si/al, na/al molar ratios and free water on micromorphology and macro-strength of metakaolin-based geopolymer, Materials 14 (2021), https://doi.org/10.3390/ma14143845.
[48] N. Belmokhtar, L. Ben, S. Lamrani, Effect of Na 2 SiO 3 /NaOH mass ratio on the development of structure of an industrial waste-based geopolymer, J. Mater. Environ. Sci. 7 (2016) 390–396.
[49] H. Castillo, H. Collado, T. Droguett, S. Sánchez, M. Vesely, P. Garrido, S. Palma, Factors affecting the compressive strength of geopolymers: a review, Minerals 11 (2021), https://doi.org/10.3390/min11121317.
[50] S. DeMeo, Revisiting molar mass, atomic mass, and mass number: organizing, integrating, and sequencing fundamental chemical concepts, J. Chem. Educ. 83 (2006) 617.
[51] Y. Ling, K. Wang, W. Li, G. Shi, P. Lu, Effect of slag on the mechanical properties and bond strength of fly ash-based engineered geopolymer composites, Compos. B Eng. 164 (2019) 747–757, https://doi.org/10.1016/J.COMPOSITESB.2019.01.092.
[52] A. Favier, G. Habert, J.B. D'Espinose De Lacaillerie, N. Roussel, Mechanical properties and compositional heterogeneities of fresh geopolymer pastes, Cem. Concr. Res. 48 (2013) 9–16, https://doi.org/10.1016/J.CEMCONRES.2013.02.001.
[53] Standard Test Methods for Compressive Strength of Chemical-Resistant Mortars, Grouts, Monolithic Surfacings, and Polymer Concretes 1, n.d. ⟨www.astm.org⟩,.
[54] Standard Test Methods for Compressive Strength of Chemical-Resistant Mortars, Grouts, Monolithic Surfacings, and Polymer Concretes 1, n.d. ⟨www.astm.org⟩,.

[55] J. Serra, P. González, S. Liste, C. Serra, S. Chiussi, B. León, M. Pérez-Amor, H.O. Ylänen, M. Hupa, FTIR and XPS studies of bioactive silica based glasses, J. Non Cryst. Solids 332 (2003) 20–27, https://doi.org/10.1016/j.jnoncrysol.2003.09.013.
[56] Y. Xi, N. Zhu, J. Huang, X. Li, W. Shen, P. Wu, Na2O induced stable heavy metal silicates phase transformation and glass network depolymerization, J. Clean. Prod. 380 (2022) 135009, https://doi.org/10.1016/J.JCLEPRO.2022.135009.
[57] R.A. Gado, M. Hebda, M. Łach, J. Mikuła, Alkali activation of waste clay bricks: influence of the silica modulus, SiO2/Na2O, H2O/Na2O molar ratio, and liquid/solid ratio, Materials 13 (2020), https://doi.org/10.3390/ma13020383.
[58] D. Lago, G. Tameni, F. Zorzi, J. Kraxner, D. Galusek, E. Bernardo, Novel cesium immobilization by alkali activation and cold consolidation of waste pharmaceutical glass, J. Clean. Prod. 461 (2024) 142673, https://doi.org/10.1016/J.JCLEPRO.2024.142673.
[59] K. Shirai, The total energy approach for calculating the specific heat of liquids and glasses, J. Phys. Condens. Matter 37 (2025) 473008.
[60] P. Bajpai, Basic overview of pulp and paper manufacturing process, Green. Chem. Sustain. Pulp Pap. Ind. 10 (2015) 11–39, https://doi.org/10.1007/978-3-319-18744-0_2.
[61] E. Adesanya, K. Ohenoja, A. Di Maria, P. Kinnunen, M. Illikainen, Alternative alkali-activator from steel-making waste for one-part alkali-activated slag, J. Clean. Prod. 274 (2020) 123020, https://doi.org/10.1016/J.JCLEPRO.2020.123020.
[62] P.J. Ardhira, S.K. Shukla, D. Sathyan, Synthesis of geopolymer mortar from biomass ashes and forecasting its compressive strength behaviour, Case Stud. Constr. Mater. 21 (2024) e03581, https://doi.org/10.1016/J.CSCM.2024.E03581.
[63] A.Z.W. Wazien, M.M.A.B. Abdullah, R. Abd Razak, M.A.Z.M.R. Rozainy, M.F.M. Tahir, Strength and density of geopolymer mortar cured at ambient temperature for use as repair material, in: IOP Conf. Ser. Mater. Sci. Eng., Institute of Physics Publishing, 2016, https://doi.org/10.1088/1757-899X/133/1/012042.
[64] S.H. Teh, T. Wiedmann, A. Castel, J. de Burgh, Hybrid life cycle assessment of greenhouse gas emissions from cement, concrete and geopolymer concrete in Australia, J. Clean. Prod. 152 (2017) 312–320, https://doi.org/10.1016/J.JCLEPRO.2017.03.122.
[65] B.C. McLellan, R.P. Williams, J. Lay, A. Van Riessen, G.D. Corder, Costs and carbon emissions for geopolymer pastes in comparison to ordinary portland cement, J. Clean. Prod. 19 (2011) 1080–1090, https://doi.org/10.1016/J.JCLEPRO.2011.02.010.
[66] A.A. Setiawan, H. Hardjasaputra, R. Soegiarso, Embodied carbon dioxide of fly ash based geopolymer concrete. IOP Conf. Ser. Earth Environ. Sci., Institute of Physics, 2023, https://doi.org/10.1088/1755-1315/1195/1/012031.
[67] M. Abdulkareem, J. Havukainen, J. Nuortila-Jokinen, M. Horttanainen, Environmental and economic perspective of waste-derived activators on alkali-activated mortars, J. Clean. Prod. 280 (2021) 124651, https://doi.org/10.1016/J.JCLEPRO.2020.124651.
[68] K. Neupane, Evaluation of environmental sustainability of one-part geopolymer binder concrete, Clean. Mater. 6 (2022) 100138, https://doi.org/10.1016/J.CLEMA.2022.100138.
[69] D. Sinkhonde, T. Bezabih, On the computational evaluation of carbon dioxide emissions of concrete mixes incorporating waste materials: a strength-based approach, Clean. Waste Syst. 8 (2024) 100149, https://doi.org/10.1016/J.CLWAS.2024.100149.